An International Journal of Optimization and Control: Theories & Applications
ISSN: 2146-0957 eISSN: 2146-5703
Vol.16, No.2, pp.478-498 (2026)
https://doi.org/10.36922/IJOCTA025440185

RESEARCH ARTICLE

Response control of buoyant leg storage and regasification platform using magnetorheological dampers

Shyba Arakkan[1,2] and Srinivasan Chandrasekaran[1*]

[1]Department of Ocean Engineering, Indian Institute of Technology Madras, Chennai, Tamil Nadu, India
[2]Department of Civil Engineering, Government Engineering College Kozhikode, Kozhikode, Kerala, India
drsekaran@iitm.ac.in, oe23d010@smail.iitm.ac.in

ARTICLE INFO

Article History:
Received: October 29, 2025
Revised: November 28, 2025
Accepted: December 10, 2025
Published online: January 8, 2026

Keywords:
Buoyant leg storage and regasification platform
Bouc–Wen model
Magneto-rheological damper
Regasification
Semi-active control

AMS Classification 2010:
76M12; 76R10; 80A20; 76D05; 65N30

ABSTRACT

The rising demand for liquefied natural gas (LNG) has spurred research into offshore regasification platforms as a reliable solution to meet global energy needs. Buoyant leg storage and regasification platforms (BLSRPs) offer superior positional stability compared to ship-shaped alternatives; however, heave motion needs to be mitigated for safe regasification. This study proposes a semi-active response control mechanism (RCM) employing magnetorheological (MR) dampers to suppress radial buoyant leg displacements, which are directly coupled with deck heave. A baseline numerical model of the BLSRP was developed in AQWA software without an RCM, and a mathematical model incorporating the MR-RCM was formulated to evaluate the controlled system performance. Unlike previous BLSRP studies, we explicitly incorporated combined wave–wind–current environmental loading conditions. Transformation matrices were established to convert radial responses into deck heave, with influence factors calibrated for varying sea states and approach angles. Results indicate that the MR-RCM achieves 30–45% root-mean-square reductions in radial displacements under moderate and high sea conditions, resulting in significant control of deck heave. Even under very high sea states, 8–11% reductions are maintained, preventing uncontrolled escalation. Hysteresis plots validate the nonlinear energy dissipation of MR dampers and their adaptability to broadband excitations. The findings demonstrate that MR-RCM improves platform stability, reduces boil-off gas generation, and enhances safety in LNG operations. Overall, the study establishes MR-based semi-active damping as a practical and scalable solution for offshore platforms, bridging the limitations of passive devices and the complexities of fully active systems.

1. Introduction

Recent developments in offshore platforms have expanded operational capability in deep and ultra-deep waters. Offshore regasification plays a critical role in the liquefied natural gas (LNG) supply chain by converting LNG at cryogenic temperatures into natural gas. Compared to onshore LNG terminals, offshore regasification reduces infrastructure needs and offers deployment flexibility in regions lacking land-based facilities.[1–3] Floating storage and regasification units (FSRUs) are currently the most widely used solution; however, these mobile units face challenges, including high operational cost, site restrictions, and complex risk-mitigation requirements.[4,5] As LNG demand grows, safety concerns have become critical, reinforced by structural integrity and mooring standards prescribed by international classification societies.[6,7] Safety analysis of high-pressure

*Corresponding Author

fuel gas systems in LNG-powered marine applications highlights the operational sensitivity and design complexity of regasification infrastructure.[8]

Among other alternatives, the new buoyant leg storage and regasification platform (BLSRP) has emerged as a promising solution. The BLSRP can be deployed as a supplementary platform near an LNG exploration field to conduct offshore regasification. Unlike FSRUs, the BLSRP benefits from a form-dominant geometry that improves restoring forces and load distribution. Both experimental and numerical studies confirm its superior performance.[9,10] Investigations under eccentric loading further reveal Mathieu-type stability, confirming operational feasibility in varying sea states.[11] However, managing dynamic responses remains a challenge. Excessive heave, roll, and pitch under irregular waves compromise regasification stability, increase boil-off gas (BOG) generation, and elevate vapor cloud and fire risks.[12] While hinged deck–leg connections partially isolate motions, they are insufficient during extreme loading, tether failures, or asymmetric LNG transfer. Therefore, additional response control mechanisms (RCMs) are required.

Advanced supplementary damping systems have been shown to enhance dynamic stability in large structural systems.[13] Passive control devices are commonly preferred for response mitigation due to their simplicity and robustness. Tuned mass dampers, tuned liquid column dampers, and linear spring isolators shift frequencies or dissipate energy through controlled stiffness and damping.[14–17] Linear spring-based systems are valued for low cost, easy implementation, and reduced maintenance, while still achieving meaningful response mitigation.[18,19] These devices improve operational stability and extend structural life, but their fixed characteristics restrict adaptability across sea states, limiting effectiveness during critical regasification operations. Semi-active control systems overcome this limitation by combining the benefits of passive systems with the adaptability of active control.[20]

The recent magneto-rheological (MR) damper designs, configurations, and applications have been well documented in the literature.[21] Recent reviews provide a comprehensive overview of the historical development, design principles, and modern applications of MR dampers, providing important insights into recent technological trends in MR-based vibration control.[22] MR dampers use smart fluids whose viscosity changes under a magnetic field, producing controllable damping forces.[23,24] Unlike active systems, they consume low energy while maintaining adaptability. Their nonlinear hysteretic behavior is well captured by the Bouc–Wen model, representing elastic and post-yield characteristics with computational efficiency.[25–27] Compared to Bingham, Dahl, and other modified hysteresis models, Bouc–Wen offers greater flexibility in reproducing symmetrical and non-symmetrical loops.[28] Other MR models, namely Bingham plastic, Herschel–Bulkley, Spencer, and neural network approaches, offer varying trade-offs between complexity and accuracy.[29] However, Bouc–Wen remains the most widely adopted due to its adaptability and efficiency.[25]

The potential of MR dampers in offshore applications has been increasingly demonstrated. Jacket-type platforms showed significant suppression of structural responses under combined wave and wind excitation.[30,31] Hybrid devices, such as MR-tuned liquid column gas dampers, extend bandwidth by integrating fluid damping with MR adaptability. Nonlinear isolator studies confirm improved vibration suppression over passive devices.[32] Semi-active energy-based control laws further enhance broadband stability.[33] Applications across large civil structures also verify MR adaptability to full-scale systems.[34,35] Despite these advances, studies specific to BLSRP remain limited. The present work addresses this gap by developing a numerical model for dynamic analysis with the MR damper. The BLSRP model was created in AQWA software (2024 R2, ANSYS, Inc., United States of America) to capture buoyant leg radial motions under combined wave, wind, and current loads. These radial displacements were targeted for MR-based control, as they directly coupled with deck heave. The proposed MR-RCM reduced the heave response by mitigating radial leg motions, enhancing operational stability. The approach integrated energy dissipation capacity with adaptability to irregular excitations, ensuring reliability during normal and extreme sea states. The MR-RCM framework advances compliant offshore platform design by bridging the gap between passive limitations and active complexities. By applying semi-active damping to BLSRP, the study establishes a scalable solution for safe and efficient offshore regasification operations.

2. Methodology

A numerical analysis of the BLSRP was performed in AQWA software, without an RCM, to investigate platform response under varying sea

states, using geometrical and structural parameters reported by Chandrasekaran and Lognath.[9] The platform comprised a circular deck supported by buoyant legs symmetrically arranged and connected through hinges, allowing radial rotation in the vertical plane for inward and outward motion, while tethers maintained the position (**Figure 1**). Each leg was fitted with an MR-RCM, linked via a pin joint at one end and attached to the deck's central shaft through a connection plate at the other. The pin ensured the damper remained horizontal despite radial leg motions.

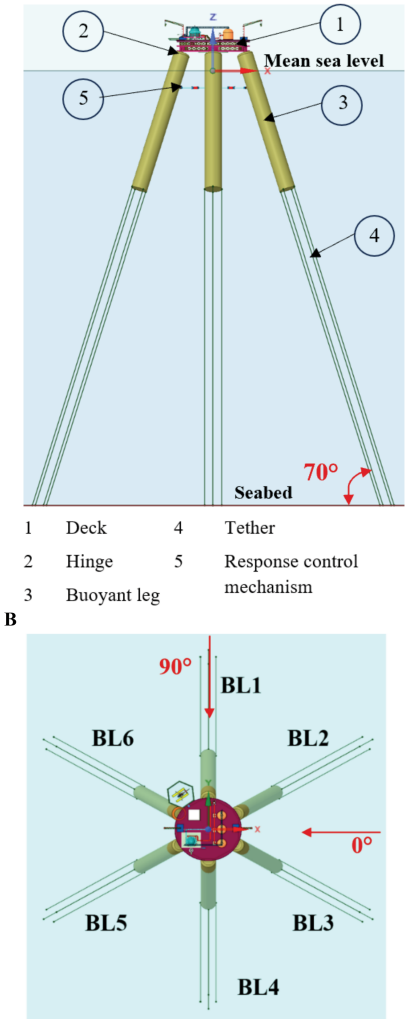

Figure 1. Buoyant leg storage and regasification platform with response control mechanism. (A) Front view. (B) Top view.
Abbreviation: BL: Buoyant buoyant leg.

Figure 2 illustrates the main platform elements, including cranes, service decks, a helipad, and living quarters. LNG is stored in cryogenic tanks at –162 °C to maintain a liquid state. Heat input during operations causes partial evaporation, generating BOG, which is typically reliquefied or used as fuel. Regasification is achieved by circulating seawater through pipelines to specialized heat exchangers, where it serves as a heat source to convert LNG into natural gas. Efficient BOG recondensation can significantly enhance regasification performance and energy utilization.[36]

Alternative placement options for the MR-RCM, such as horizontal bracing-mounted dampers and mid-leg configurations, were initially examined. As the motion of the buoyant leg is radial to the center of the deck, the leg–deck joint was selected because it provides maximum mechanical leverage per unit damper stroke and minimal interference with LNG process equipment, making it the most effective and constructible location.

3. Numerical analysis without magneto-rheological response control mechanisms

3.1. Model development

The platform geometry was developed in Design Modeler (2024 R2, ANSYS Inc., United States of America), with the circular deck modeled as a solid element and the buoyant legs represented as a tube element. The structural parameters are listed in **Table 1**. The legs were connected to the deck through hinge joints, allowing rotation about the local x-axis of the hinge while ensuring symmetric motion about the vertical axis. Each leg was secured to the seabed using four parallel tethers of varying lengths but subjected to the same pretension. Mass and inertia properties were appropriately defined to complete the model.[35,37] The topside structures were simplified for numerical analysis into equivalent representative forms to minimize computational effort, as shown in **Figure 3**.

The static equilibrium of the structure, with tether pretension and buoyancy, is given by **Equation** (1):

$$F_b = W + N\ T_0\ sin\theta \tag{1}$$

where F_b denotes the buoyancy force, W is the platform weight without the RCM, N is the number of buoyant legs, T_0 is the tether pretension, and θ is the leg inclination to the vertical.

3.2. Sea conditions

The study considered three sea states—moderate, high, and very high, representing normal operations, storms, and extreme survival scenarios. Irregular waves were modeled using the Joint North Sea Wave Project (JONSWAP) spectrum, while current effects followed a three-point Gulf of Mexico profile as per Det Norske Veritas (DNV) Recommended Practice C205.[7]

Wind loads were estimated using offshore power-law and gust factors, in accordance with

Table 1. Structural parameters

Parameter	**Dimensions**
Diameter of the deck	100 m
Diameter of the buoyant legs	22.50 m
Number of buoyant legs	6
Water depth	600 m
Mass of the structure (without RCM)	4×10^8 kg
Mass of RCM	3.750×10^6 kg
Length of MR assembly	44.59 m
Depth of MR assembly from the mean sea level	26.64 m
Free board	24.37 m
Mass of deck	4.055×10^7 kg
Center of mass of the deck	0.477 m; −0.440 m; 41.072 m
Mass of buoyant legs	2.550×10^7 kg
Ballast	3.340×10^8 kg
Meta-center without RCM	17.763 m
Meta-center with RCM	17.587 m
Length of the buoyant leg	200 m
Draft	163.57 m
Modulus of elasticity of tether	2.1×10^{11} N/m^2
Length of tether for each buoyant leg	455.02 m; 451.17 m; 447.17 m; and 451.17 m
Tether stiffness	875741 N/m

Abbreviations: MR: Magnetomagneto-rheological; RCM: Response response control mechanism.

Table 2. Sea states

Sea state	**Moderate**	**High**	**Very high**
Significant wave height, H_s (m)	6.50	10.00	15.00
Zeo crossing wave period, T_z (s)	8.15	10.00	15.00
Wind speed at 10 m height, V_{10} (m/s)	15.00	35.00	45.00

Table 3. Summary of sea states and environmental conditions

Sea condition	Approach angle	RCM status	Sea state
Wave + current + wind	(i) 0° (ii) 90°	(i) With RCM (ii) With-out RCM	(i) Moder-ate (ii) High (iii) Very high

Abbreviation: RCM: Response response control mechanism.

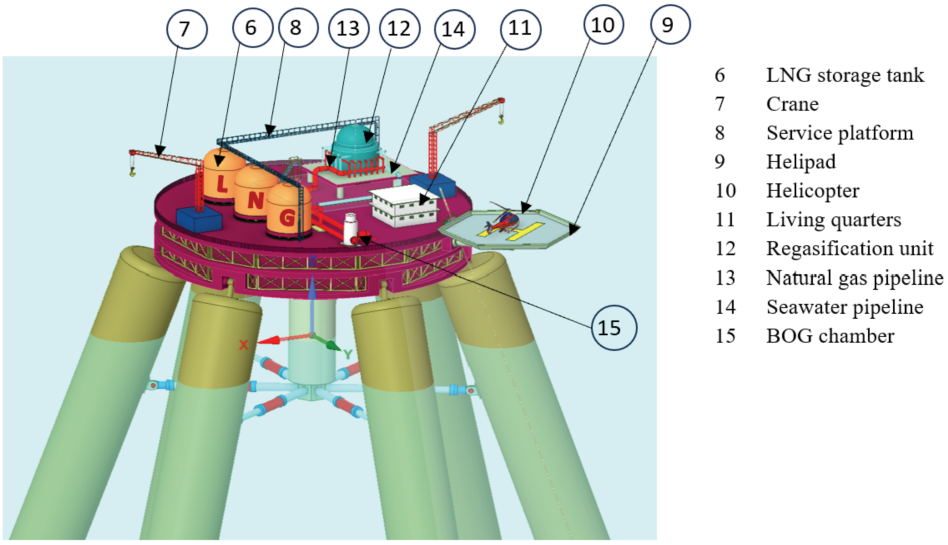

Figure 2. Conceptual model of buoyant leg storage and regasification platform with magneto-rheological response control mechanism (Patented).
Abbreviations: BOG: Boilboil-off gas; LNG: Liquefied liquefied natural gas

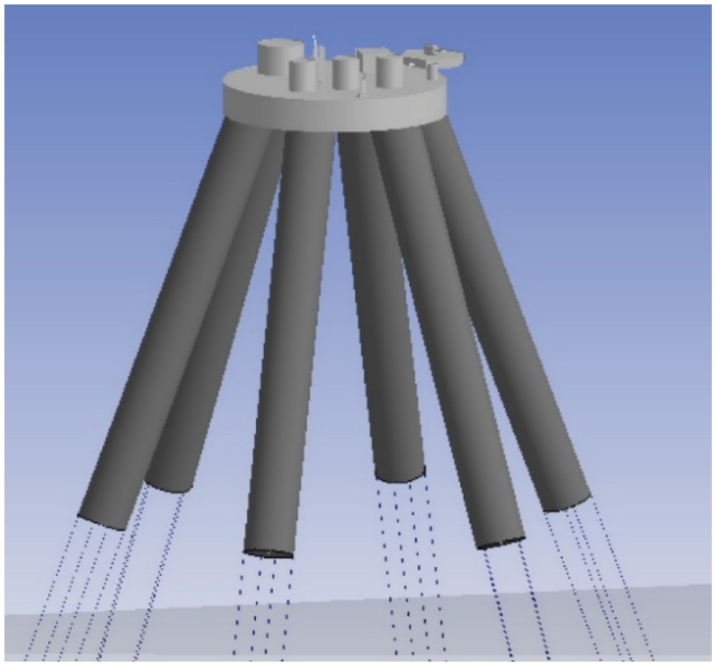

Figure 3. Numerical model of buoyant leg storage and regasification platform without magneto-rheological response control mechanisms

American Petroleum Institute and DNV guidelines. These environmental inputs allowed a realistic assessment of BLSRP dynamics, enabling comparison of heave responses with and without MR-RCM at 0° and 90° wave approach angles to evaluate control effectiveness **(Section S2)**.

Tables 2 and 3 summarize the environmental scenarios considered for offshore platform analysis. Each case includes two wave approach angles (0° and 90°) across the sea states.

4. Semi-active control mechanism

In offshore environments, large environmental loads demand efficient vibration control without high power consumption and complexity of active systems. Through real-time adaptability, semi-active devices address this by enhancing structural safety and serviceability under varying sea states. MR dampers have gained importance, employing MR fluid to generate controllable damping forces. From a rheological perspective, MR fluid behaves as a Bingham plastic, exhibiting low

resistance without a magnetic field but transitioning rapidly to a semi-solid state with controllable yield stress when exposed to a magnetic field. This tunable rheology enables damping to be continuously adjusted between viscous and solid-like behavior within milliseconds. MR fluid consists of micron-sized ferrous particles suspended in carrier liquids, such as mineral oil, silicone oil, or synthetic oils.[38] Silicone oil offers a superior viscosity index, lower friction, and higher thermal stability, making it suitable for demanding vibration control. The main advantages of MR dampers are their high adaptability, low energy requirements, and operational reliability. They combine the robustness of passive devices with the flexibility of controllable damping, avoiding the complexity of fully active systems. Under a magnetic field, suspended particles align along field lines in chain-like structures (**Figure 4**), increasing viscosity and transforming the fluid into a semi-solid state, thereby significantly enhancing vibration control in offshore platforms.

5. Modeling of a semi-active control mechanism

When the buoyant leg of the BLSRP moves inward or outward, the MR damper resists this motion by forcing the MR fluid to flow through a fluid channel. The applied magnetic field alters the fluid's yield stress, enabling the damper to instantly adjust its resistance based on the leg's displacement direction and velocity. As a result, inward and outward motions are controlled adaptively, dissipating energy while preventing excessive radial leg movement. **Figure 5A** shows the MR-RCM, where dampers are symmetrically mounted on each leg to regulate inward and outward radial motions. The exploded view (**Figure 5B**) shows the main damper components—piston, casing, and electromagnetic coil that provide variable resistance under a magnetic field. The sectional view in **Figure 6** illustrates piston movement forcing MR fluid through a gap, where its rheology is tuned in real time to dissipate energy and suppress leg motion. This arrangement ensures adaptive response control and maintains LNG platform stability under dynamic sea loads.

Each buoyant leg is equipped with a linear variable differential transformer positioned near the damper–pin joint along the radial axis, enabling accurate inward–outward motion capture for real-time control feedback.

The mooring system is modeled as a taut, highly pretensioned configuration typical of BLSRPs. Although the MR-RCM introduces an equivalent mass of 3.75×10^6 kg, which is nearly 0.94% of the structural weight of the platform, its design ensures that the actual and equivalent volumetric displacements are identical, making the assembly neutrally buoyant. This prevents any change in hydrostatic restoring forces, tether pretension, or global equilibrium. Accordingly, the interaction between MR damper forces and mooring tension remains minimal under normal and high sea states, allowing the control mechanism to focus on suppressing radial leg motion without disturbing pretensioned tether behavior.

Under very high sea conditions, the increased heave response keeps the mooring lines fully stretched, and the mooring system becomes the dominant contributor to overall stability. In this regime, the MR-RCM shifts from enhancing performance to preventing uncontrolled escalation, which explains the reduced control effectiveness during extreme events.

Economically, the neutrally buoyant configuration eliminates the need for added buoyancy tanks, ballast modifications, or structural reinforcements. The MR-RCM fits within existing construction phases without increasing hydrodynamic loading or altering platform hydrostatics.

In the BLSRP, each buoyant leg moves radially outward from the deck center, not directly aligned with global surge and sway responses. Only buoyant legs (BLs) 1 and 4 coincide with the global sway degree of freedom. As MR dampers are oriented radially, their force depends on displacement and velocity along the leg's radial axis. Wave, wind, and current loads induce oscillations at hinge connections, resulting in radial displacements relative to the deck. The damper generates restoring and dissipative forces proportional to this radial motion, making the radial displacement of each leg the most appropriate performance measure. To capture this, global surge and sway components are projected onto each leg's radial axis, as shown in **Figure 7**. Controlling inward–outward radial displacements indirectly reduces deck heave and enhances overall platform stability. The global surge and sway to radial displacement in general form is given in **Equation** (2):

$$r_{BLi}=cos(\theta_{BLi})BL_{i,\ surge}+sin(\theta_{BLi})BL_{i,sway} \quad (2)$$

where $i = 1$ to –6. Here, $\boldsymbol{BL_{i,\ surge}}$ and $\boldsymbol{BL_{i,\ sway}}$ are taken in the opposite direction of the global surge to define the radial inward (towards the center) of the deck, and $\boldsymbol{\theta_{BLi}}$ is the leg angle in the horizontal plane measured from the global surge (positive) axis in the counterclockwise direction.

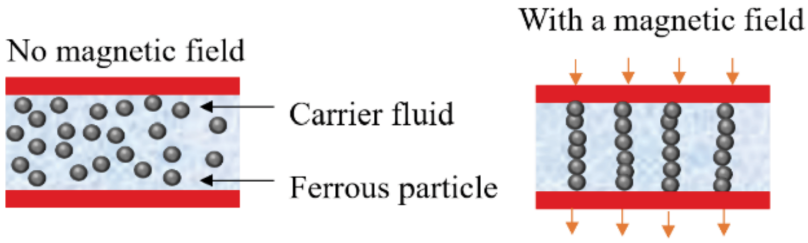

Figure 4. Mechanism of the magneto-rheological damper

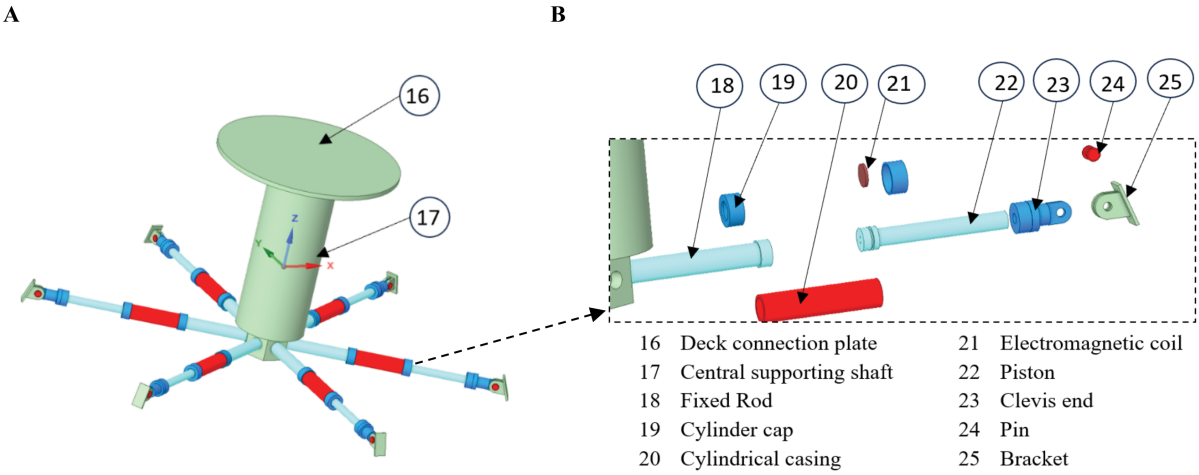

Figure 5. Magneto-rheological damper assembly. (A) Working mechanism. (B) Exploded view

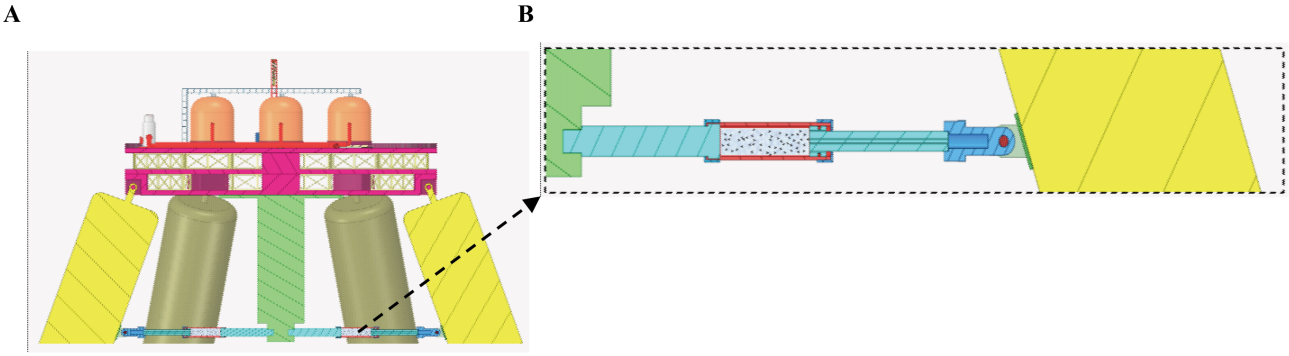

Figure 6. Magneto-rheological response control mechanism. (A) Vertical cross-section. (B) Enlarged view of the magneto-rheological assembly

From the top view of the BLSRP, the following angles can be measured: $\theta_{BL1} = 90°$, $\theta_{BL2} = 30°$, $\theta_{BL3} = -30°$, $\theta_{BL4} = -90°$, $\theta_{BL5} = -150°$, and $\theta_{BL6} = 150°$.

Figure 8 presents a hysteresis loop of an MR damper using the Bouc–Wen model for one cycle of energy dissipation. The model captures nonlinear force–displacement behavior, governed by current-induced magnetic fields that alter MR fluid properties and energy dissipation. It effectively represents elastic stiffness, hysteretic loops, viscous effects, and smooth transitions between pre- and post-yield states, making it well-suited for simulating MR dampers in semi-active control applications.

5.1. Equations of motion for one buoyant leg

Let $x(t)$ be the small radial displacement of the leg at the joint connecting the MR assembly to the buoyant leg with a pin connection. Consider the line of action radially towards the deck center as positive. The effective mass in this radial direction is given by **Equation (3)**:

$$m_e = m_{st} + m_a \tag{3}$$

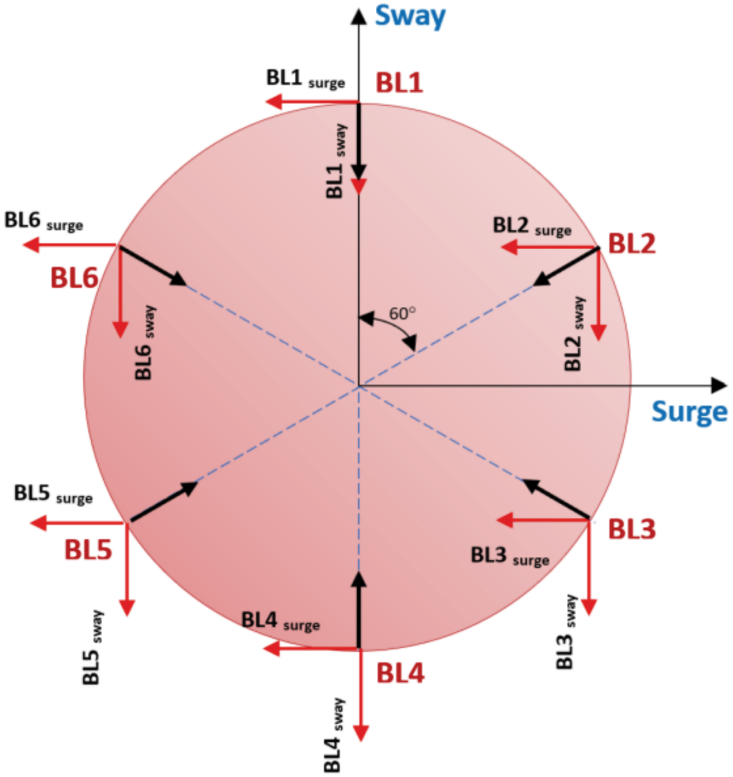

Figure 7. Global surge and sway to local radial displacement transformation. Abbreviation: BL: Buoyant buoyant leg

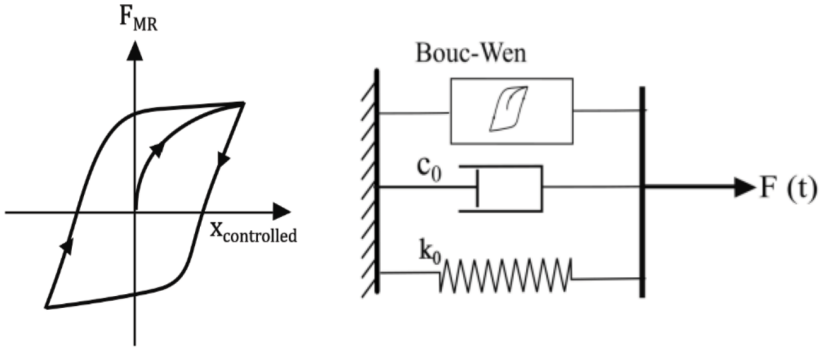

Figure 8. Bouc–Wen model of magneto-rheological damper

where, m_{st} and m_a are the structural and added masses of the buoyant leg, respectively.

Similarly, the effective damping in the radial direction is given by **Equation (4)**:

$$c_e = c_{st} + c_{rad} \quad (4)$$

where, c_{st} and c_{rad} are the structural and radiational damping of the buoyant leg, respectively. The effective stiffness of the buoyant leg is given in **Equation (5)**:

$$k_e = k_{leg} + k_{hyd} \quad (5)$$

where k_{leg} and k_{hyd} are the stiffness of the leg and the hydrodynamic stiffness, respectively.

By considering a single buoyant leg, the equation of motion is given as in **Equation (6)**:

$$m_e\ddot{x}(t) + c_e\dot{x}(t) + k_e x(t) + F_{MR}(t) = F_{ext}(t) \quad (6)$$

For a slight rotation about the hinge connection, the radial displacement and radial velocity at the pin are $x \cong r\emptyset$ and $\dot{x} \cong r\dot{\emptyset}$, where r is the perpendicular lever arm from the hinge to the MR pin measured normal to the damper axis. $F_{ext}(t)$ is the externally transmitted excitation along the leg's radial axis. The MR damper force is modeled with Bouc–Wen hysteresis as shown in **Equation (7)**:

$$F_{MR}(t) = \alpha k_e x(t) + (1-\alpha)\ k\ z(t) + c_0\dot{x}(t) \quad (7)$$

The first term in **Equation (7)** denotes the elastic restoring force proportional to displacement, with α defining the share of total stiffness contributed by this elastic component. The second term represents the hysteretic restoring force, where $z(t)$ is the internal variable that captures memory-dependent nonlinear effects and energy dissipation through hysteresis. The third term is the viscous damping force, proportional to velocity, accounting for time-dependent energy loss. MR fluid particles experience greater shear at higher velocities, strengthening the pinching effect. Together, these three forces constitute the MR damping force.

The Bouc–Wen parameter ranges were initially selected based on experimentally validated identification studies on large-capacity MR dampers reported for offshore and civil structures.[39–42] The parameters were then tuned numerically so that the simulated force–displacement hysteresis loops fall within the practical damper force capacity corresponding to buoyant leg radial loads. Although BLSRP-specific laboratory tests are not available at this stage, the adopted calibration ensures realistic stiffness, hysteresis energy, and post-yield slope. Experimental validation of MR-RCM parameters under BLSRP-scale loads is planned as future work.

The coefficient (α) balances elastic and hysteretic stiffness, influencing energy storage versus dissipation. Parameters (β, γ) govern loop smoothness, pinching, and symmetry, dictating hardening or softening behavior. A scale the linear contribution to hysteresis evolution, while exponent n sharpens the transition between elastic and post-yield phases. The parameter ranges and selected values used for analysis are provided in **Table 4**.

The mathematical formulation of a hysteretic variable $\dot{z}(t)$ is given by **Equation (8)**:

$$\dot{z}(t) = A\,\dot{x}(t) - \beta\,|\dot{x}(t)|\,|z|^{n-1}z - \gamma\,\dot{x}(t)\,|z|^{n} \tag{8}$$

where $\dot{x}(t)$ represents the velocity of the damper. $z(t)$ and $\dot{z}(t)$ do not directly represent a displacement or velocity, but it tracks the memory effect of the damper. The first term ensures the hysteretic variable evolves with velocity as input and scales the linear contribution with the factor A. The second term controls the smoothness and pinching of the hysteresis loop. It depends on the present velocity magnitude and the present state of hysteresis. The term ensures that the greater the damper's yield, the stronger the restoring force. A large value of gives a stronger restoring effect, making the loop smoother and stable. The $|\dot{x}(t)|$ ensures that the term always acts as an energy-dissipating effect, independent of whether the leg is moving forward or backward. $|z|^{n-1}$ ensures the restoring force grows consistently with the magnitude of hysteresis. The third term controls the asymmetry of the hysteresis loop, while n governs the sharpness of the transition from elastic to post-yield behavior.

5.2. Practical considerations

Generally, the MR-RCM is designed for long-term use with stabilized MR fluid and static multi-stage seals that are highly durable and withstand a large number of loading cycles.[43] Scheduled maintenance can be aligned with the servicing cycle of regasification platforms, and the modular MR-RCM layout allows individual unit replacement by temporarily locking the hinge connection, and thereby pausing the buoyant leg for a short period, without interrupting platform operation. A detailed techno-economic evaluation of long-term operational savings is proposed for future work.

5.3. Real-time control implementation and sensing requirements

With dominant platform periods between 8.15 s and 15 s, the highest structural excitation frequency is about 0.123 Hz. A 50 Hz sampling rate (0.02 s interval) oversamples this frequency by a factor of more than 400, thereby avoiding misidentification and minimizing digital delay. The corresponding phase lag is less than 1°, which is negligible for a slow offshore structure. Thus, a control update rate of at least 50 Hz is sufficient for effective real-time MR-RCM operation (**Section S1**).

5.4. Buoyant leg radial displacement to deck heave transformation

The primary objective of this study is the effective control of deck heave. As the MR-RCM acts on buoyant legs, radial displacements are directly controlled. To connect this control to deck motion, the radial responses are transformed into deck heave, assuming inward and outward leg motions induced by environmental loads are the main contributors to vertical displacement. Thus, controlled radial responses are mapped to deck heave. **Figure 9** illustrates this transformation.

The hinged deck–leg joint ensures that only the radial in–out motion of each buoyant leg is transmitted to the MR dampers, while bending

Table 4. Parameters of the numerical model[39–42]

Parameter	Description	Typical range	Valued used
α	Ratio of elastic to hysteretic stiffness (influences the balance between energy storage and dissipation)	0.0–1.0	0.4
β	Controls loop smoothness and pinching	0.1–0.5	0.5
γ	Controls the asymmetry of the loop	0.5–1.0	0.5
A	Scale of linear contribution in hysteresis evolution	0.5–1.0	1.0
n	Sharpness of transition	1.0–5.0	5.0
k_{bw}	Post-yield stiffness of damper [(N/m)]	10^6–10^{10}	1.09×10^7
c_0	Viscous damping [(N·s/m)]	10^3–10^6	2.00×10^6

moments are filtered out. Because the hinge eliminates moment transfer, leg rotation does not influence deck heave or damper stroke, making radial displacement the dominant kinematic degree of freedom in the system. This simplifies the control implementation, since the numerical model needs to track only the radial component of leg motion. The surge–sway to radial transformation naturally captures this behavior, as the hinge constrains motion to a purely radial path.

Figure 9A shows the overall BLSRP geometry with legs, hinges, and MR dampers, where external loads generate radial displacements. **Figure 9B** shows the enlarged view of the leg–deck interface, demonstrating how radial displacement X_{radial} translates into vertical deck heave. The adopted transformation procedure is as follows:

The influence factor for each leg, wi, is evaluated as in **Equation (9)**:

$$\mathrm{w}_i = \left(\frac{Heave_{\ deck,un\_cnrl}}{rad_{\ i\ leg,un\_cnrl}}\right),\ (i = 1 \text{ to } -6). \tag{9}$$

where $Heave_{\ deck,un\_cnrl}$ is the heave response of the deck and $rad_{\ i\ leg,un\_cnrl}$ is the radial displacement of each buoyant leg without RCM. The influence factor varies with each leg, sea state, and approach angle.

The transformation from radial leg displacement to deck heave is expressed in **Equation (10)**:

$$\{T\}_{6\ \times 1} = \frac{1}{6}\ \{w_i\}_{6\ \times 1} = \frac{1}{6}[w_1\ w_2\ w_3\ w_4\ w_5\ w_6]^T \tag{10}$$

Accordingly, the controlled deck heave is obtained as in **Equation** (11):

$$\begin{aligned} Heave_{\ deck,cnrl} &= [T]^T_{\ 1\ \times 6}\{r_{i,cnrl}\ \}_{6\ \times 1} \\ &= \frac{1}{6}\ [w_1\ w_2\ w_3\ w_4\ w_5\ w_6] \\ &\times [r_1\ r_2\ r_3\ r_4\ r_5\ r_6]^T_{cnrl} \end{aligned} \tag{11}$$

where $[r_1\ r_2\ r_3\ r_4\ r_5\ r_6]^T_{cnrl}$ is the controlled radial displacement of each buoyant leg. This procedure determines the influence factors for all legs and computes the controlled deck heave displacement.

6. Results and discussions

The combined action of wave, wind, and current at a 0° approach angle produced noticeable asymmetric excitations on the BLSRP. The time series plots in **Figure 10** reveal that under uncontrolled conditions, buoyant legs BL2, BL3, BL5, and BL6 underwent significant radial displacements, reaching values of 8–11 m, while BL1 and BL4 experienced smaller amplitudes of around 3 m. With the MR-RCM activated, displacements were visibly suppressed across all legs. Notably, the maximum response in BL5 and BL6 was considerably reduced, and all legs showed lower minimum responses, reflecting effective damping control.

The hysteresis loops in **Figure 11** further illustrate the nonlinear energy dissipation achieved by the MR damper. Wider loops in BL2, BL3, BL5, and BL6 corresponded to larger displacement ranges and higher energy input, whereas BL1 and BL4 displayed more compact loops, indicating efficient suppression. The plots and statistics demonstrate that MR-RCM significantly

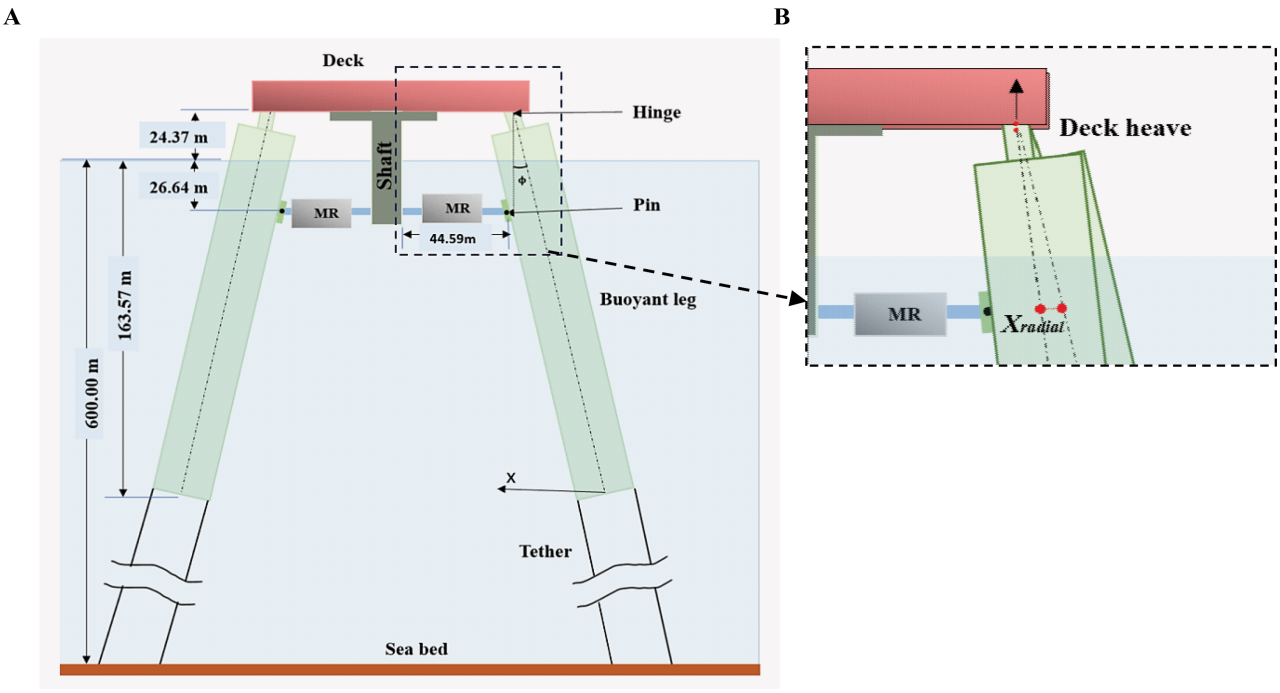

Figure 9. Kinematic relationship between buoyant-leg radial displacement and deck heave in the BLSRP. (**A**) Overall configuration showing the hinged deck–buoyant leg connection and the MR-based response control mechanism. (**B**) Enlarged view illustrating the geometric coupling between radial leg motion and vertical deck response

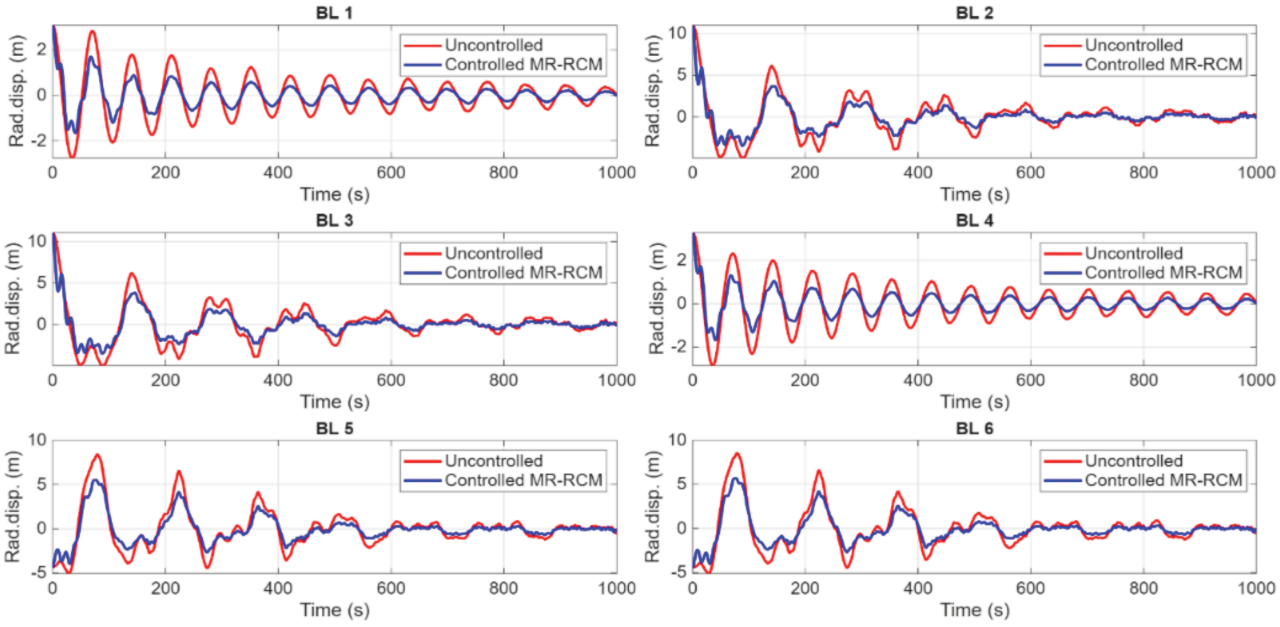

Figure 10. Radial displacement (Rad.disp.) of buoyant legs (BLs) (wave + wind + current; moderate sea state; approach angle 0°; $H_s = 6.5$ m; $T_z = 8.15$ s). Abbreviation: MR-RCM: Magnetomagneto-rheological response control mechanism

reduced motion, enhanced stability, and ensured consistent energy dissipation under moderate sea conditions.

As shown in **Figure 12**, uncontrolled responses peaked at 12 m in BL1, while BL2, BL4, and BL6 ranged between 7 and 9 m. With MR-RCM engaged, displacements were reduced, particularly in BL3 and BL5, where peak responses decreased significantly. Hysteresis plots (**Figure 13**) show wider loops in legs facing transverse loads, reflecting higher energy dissipation, while smaller motions yielded narrower yet stable loops.

Table 5 presents buoyant leg radial response statistics for an approach angle of 0° across moderate, high, and very high sea states. In moderate

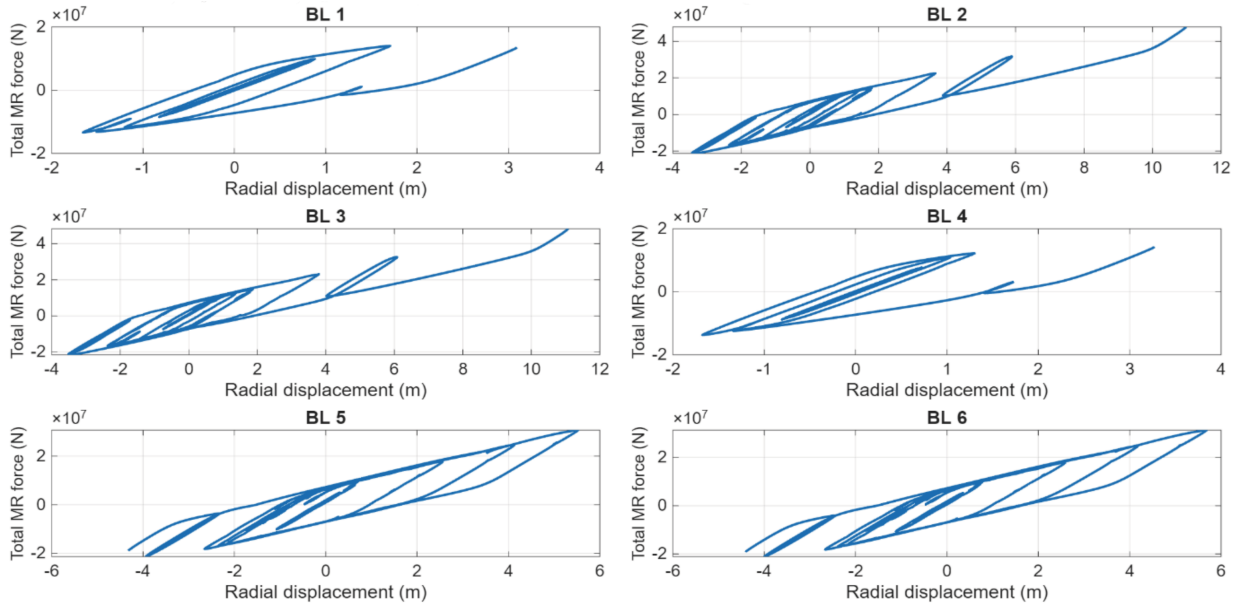

Figure 11. Hysteresis plot of buoyant legs (BLs) (wave + wind + current; moderate sea state; approach angle 0°; $H_s = 6.5$ m; $T_z = 8.15$ s).
Abbreviation: MR: Magnetomagneto-rheological.

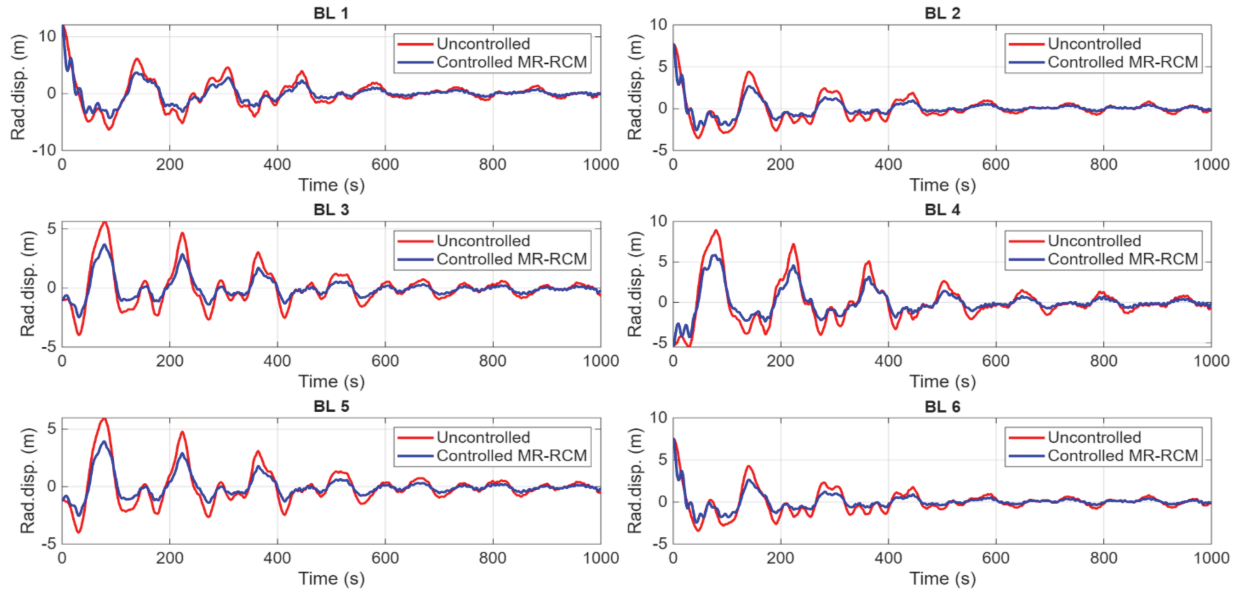

Figure 12. Radial displacement (Rad.disp.) of buoyant legs (BLs) (wave + wind + current; moderate sea state; approach angle 90°; $H_s = 6.5$ m; $T_z = 8.15$ s).
Abbreviation: MR-RCM: Magneto-rheological response control mechanism.

seas, uncontrolled root-mean-square (RMS) values ranged from 0.93 to 2.35 m, while controlled responses were reduced to 0.51–1.55 m, achieving reductions of about 32–45%. This indicates effective damping, particularly for BL1 and BL4, where reductions exceeded 44%. In high seas, leg displacements became pronounced, with uncontrolled RMS values reaching 3.06 m (BL6). Controlled values were reduced to nearly 2.07 m, with reductions in the range of approximately 30–45%. BL1 and BL4 showed maximum improvement due to their favorable orientation to wave loading. In very high seas, responses escalated sharply, with uncontrolled RMS values peaking above 3.7 m for BL2 and BL3. Control effectiveness dropped significantly, with reduction percentages below 12% for critical legs, while BL1 and BL4 still showed reductions above 40%. This suggests that MR damping retains efficiency in moderate and high seas but becomes less effective under extreme loading, where survival dominates over vibration suppression. In total, MR-RCM consistently lowered RMS values across sea states, but efficiency depended on sea severity and leg position relative

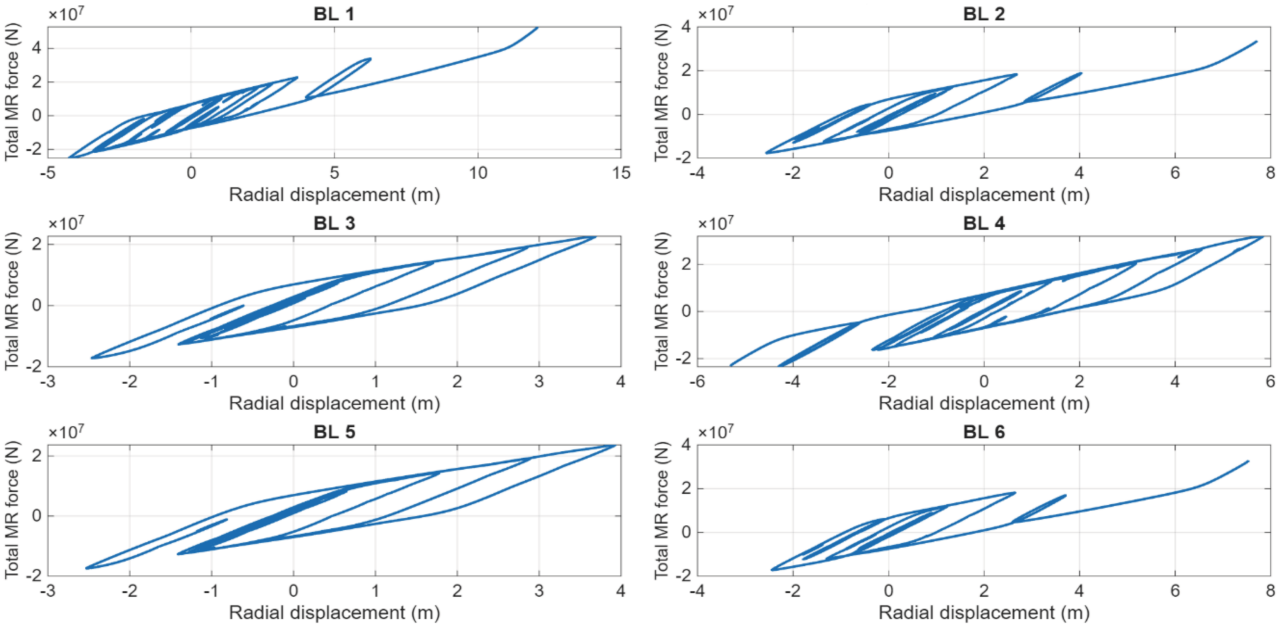

Figure 13. Hysteresis plot of buoyant legs (BLs) (wave + wind + current; moderate sea state; approach angle 90°; $H_s = 6.5$ m; $T_z = 8.15$ s).
Abbreviation: MR: Magnetomagneto-rheological.

Table 5. Buoyant leg radial response statistics (0° approach angle)

BL index	Max. (m)	Min. (m)	Mean (m)	RMS (m)	Max. (m)	Min. (m)	Mean (m)	RMS (m)	Reduction (%)
	Uncontrolled				Controlled				
Moderate sea state									
BL1	3.093	−2.760	0.000	0.930	3.093	−1.657	0.010	0.514	44.765
BL2	10.978	−4.905	0.000	2.215	10.978	−3.444	−0.024	1.501	32.256
BL3	11.070	−4.940	0.000	2.276	11.070	−3.506	−0.026	1.543	32.216
BL4	3.272	−2.851	0.000	0.938	3.272	−1.677	0.011	0.519	44.720
BL5	8.384	−5.070	0.000	2.290	5.525	−4.322	−0.066	1.509	34.110
BL6	8.535	−5.120	0.000	2.347	5.684	−4.411	−0.063	1.550	33.951
High sea state									
BL1	3.048	−2.777	0.000	0.901	3.048	−1.642	0.008	0.500	44.465
BL2	14.926	−7.243	0.000	2.911	14.926	−5.343	−0.018	2.028	30.338
BL3	15.020	−7.285	0.000	2.971	15.020	−5.401	−0.016	2.069	30.373
BL4	3.224	−2.854	0.000	0.914	3.224	−1.653	0.004	0.508	44.455
BL5	11.004	−8.054	0.000	3.003	7.216	−8.054	−0.016	2.018	32.795
BL6	11.099	−8.140	0.000	3.058	7.381	−8.140	−0.016	2.058	32.711
Very high sea state									
BL1	3.007	−2.784	0.000	0.925	3.007	−1.621	0.020	0.545	41.132
BL2	17.078	−8.920	0.000	3.662	17.078	−8.208	−0.005	3.347	8.611
BL3	17.169	−8.980	0.000	3.705	17.169	−8.316	−0.005	3.371	9.001
BL4	3.179	−2.858	0.000	0.936	3.179	−1.624	0.013	0.551	41.151
BL5	13.394	−10.4760.000		3.692	11.697	−10.4760.005		3.295	10.757
BL6	13.480	−10.5570.000		3.729	11.802	−10.5570.005		3.317	11.039

Abbreviations: BL: Buoyant buoyant leg; RMS: Root root mean square.

Table 6. Buoyant leg radial response statistics (90° approach angle)

BL index	Max. (m)	Min. (m)	Mean (m)	RMS (m)	Max. (m)	Min. (m)	Mean (m)	RMS (m)	Reduction (%)
	Uncontrolled				Controlled				
Moderate sea state									
BL1	12.091	−6.297	0.000	2.448	12.091	−4.258	0.019	1.665	31.983
BL2	7.715	−3.523	0.000	1.478	7.715	−2.560	0.054	0.978	33.849
BL3	5.641	−3.964	0.000	1.491	3.692	−2.466	−0.017	0.885	40.634
BL4	8.903	−5.501	0.000	2.485	5.840	−5.312	0.008	1.632	34.334
BL5	5.972	−3.993	0.000	1.568	3.928	−2.531	−0.006	0.944	39.782
BL6	7.542	−3.420	0.000	1.387	7.542	−2.444	0.047	0.912	34.243
High sea state									
BL1	16.665	−8.998	0.000	3.251	16.665	−5.807	−0.006	2.277	29.958
BL2	9.950	−4.299	0.000	1.812	9.950	−3.378	−0.003	1.246	31.243
BL3	7.221	−4.603	0.000	1.854	4.556	−3.240	−0.004	1.177	36.513
BL4	12.038	−9.574	0.000	3.291	7.875	−9.574	−0.008	2.230	32.236
BL5	7.461	−4.728	0.000	1.939	4.867	−3.408	−0.002	1.239	36.100
BL6	9.775	−4.194	0.000	1.719	9.775	−3.294	−0.009	1.182	31.231
Very high sea state									
BL1	19.198	−10.765	0.000	4.095	19.198	−9.886	−0.010	3.745	8.545
BL2	11.200	−5.097	0.000	2.179	11.200	−5.127	−0.006	2.086	4.277
BL3	8.721	−5.114	0.000	2.255	7.254	−5.505	0.000	2.062	8.555
BL4	14.552	−12.367	0.000	4.069	12.796	−12.367	0.007	3.656	10.144
BL5	8.935	−5.491	0.000	2.316	7.488	−5.409	0.000	2.096	9.488
BL6	11.026	−5.005	0.000	2.113	11.026	−5.139	−0.006	2.049	3.014

Abbreviations: BL: Buoyant buoyant leg; RMS: Root root mean square.

to wave attack. At a 90° approach angle under moderate sea conditions, asymmetric loading on the buoyant legs generated varied radial displacements, as reflected in the statistics summarized in **Table 6**.

Table 6 summarizes buoyant leg radial response statistics for an approach angle of 90° across moderate, high, and very high sea states. Under moderate conditions, uncontrolled RMS values ranged from 1.39 to 2.49 m, which reduced to 0.88–1.67 m after applying MR-RCM, resulting in reductions of around 32–41%. Notably, BL3 and BL5 showed the highest reductions, indicating that damping control was more effective for legs experiencing moderate but consistent excitation. In high sea states, uncontrolled RMS values rose significantly, with BL1 and BL4 exceeding 3.2 m. Controlled responses reduced them to about 2.23–2.28 m, achieving reductions of nearly 30–36%. This indicates that the MR damper provided effectiveness, although the stronger wave loads at 90° incidence led to asymmetric excitation across the legs. BL3 and BL5 showed comparatively greater percentage reductions, highlighting uneven control efficiency across loading directions and phase effects. In very high sea states, uncontrolled RMS values further escalated, with BL1 and BL4 reaching 4.10 and 4.07 m, respectively. Controlled values decreased only marginally (3.65–3.75 m), with reductions of around 8–10%. Other legs showed even lower reductions, in some cases as low as around 3%. This suggests that, under extreme conditions, damping effectiveness was significantly reduced, as structural survival dominated over control. The results indicate that MR-RCM remains effective in moderate and high seas at 90° but loses efficiency under very high sea states due to the dominance of nonlinear and extreme loading effects.

The time histories in **Figures 14** to **16** demonstrate the effect of the MR-RCM system in reducing deck heave across different sea states and approach angles. For the moderate sea state ($H_s = 6.5$ m, **Figure 14**), the controlled response tracked the uncontrolled curve closely, but with slightly reduced oscillation amplitudes, highlighting marginal improvements under low-energy input conditions. In the high sea state ($H_s = 10$ m, **Figure 15**), the benefit of control became apparent: the blue lines representing MR-RCM

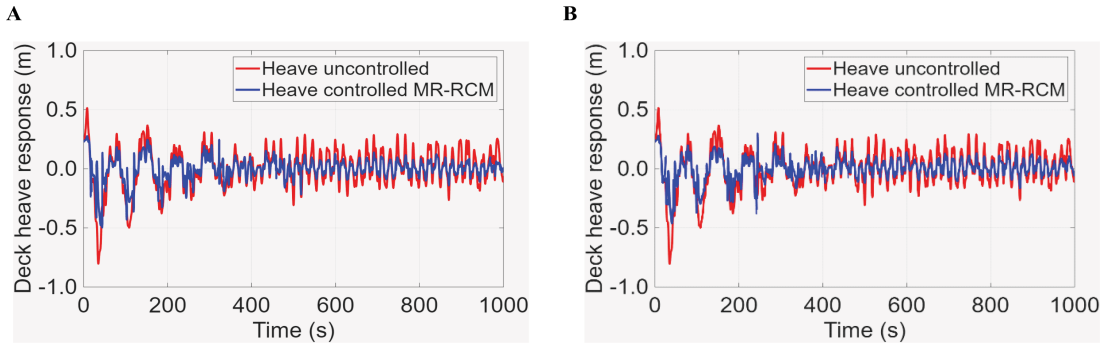

Figure 14. Heave response of deck at approach angles (A) 0° and (B) 90° (wave + wind + current; moderate sea state; $H_s = 6.5$ m; $T_z = 8.15$ s).
Abbreviation: MR-RCM: Magnetomagneto-rheological response control mechanism.

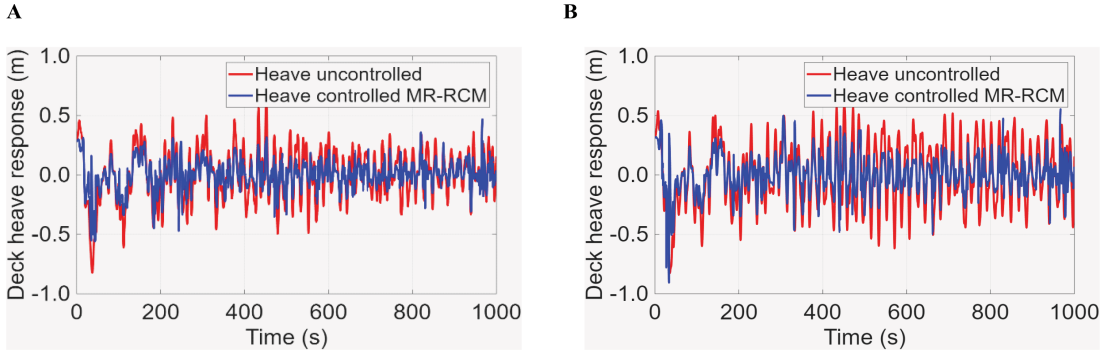

Figure 15. Heave response of deck at approach angles (A) 0° and (B) 90° (wave + wind + current; high sea state; $H_s = 10$ m; $T_z = 10$ s).
Abbreviation: MR-RCM: Magnetomagneto-rheological response control mechanism.

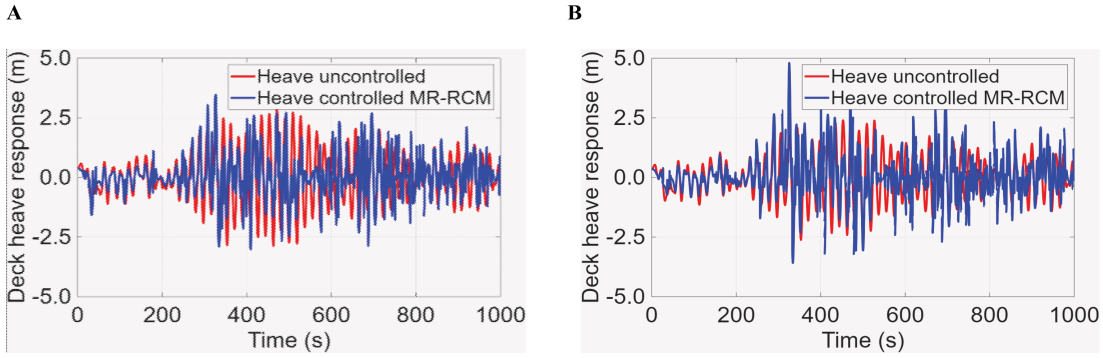

Figure 16. Heave response of deck at approach angles (A) 0° and (B) 90° (wave + wind + current; very high sea state; $H_s = 15$ m; $T_z = 15$ s).
Abbreviation: MR-RCM: Magnetomagneto-rheological response control mechanism.

show consistently narrower oscillations, particularly after 400 s, indicating enhanced damping of long-period heave. The very high sea state ($H_s =$ 15 m, **Figure 16**) illustrates the critical role of the control device: while both controlled and uncontrolled responses exhibited strong oscillations, the controlled system suppressed peak excursions, thereby preventing extreme amplitudes that could compromise structural safety.

Table 7 summarizes the statistical evaluation of the deck heave response under different sea states and approach angles. In moderate seas, RMS values were reduced by nearly 43%, indicating significant damping effectiveness of the MR-RCM. High sea states also showed substantial reductions (nearly 42%), reflecting stable control under stronger excitations. However, the reduction in very high sea states decreased to nearly 22% at 0° and $< 1\%$ at 90°, suggesting that nonlinear amplification and extreme wave loading diminished the system's efficiency. The MR-RCM demonstrated strong control in moderate to high seas, but its capability weakened under extreme conditions.

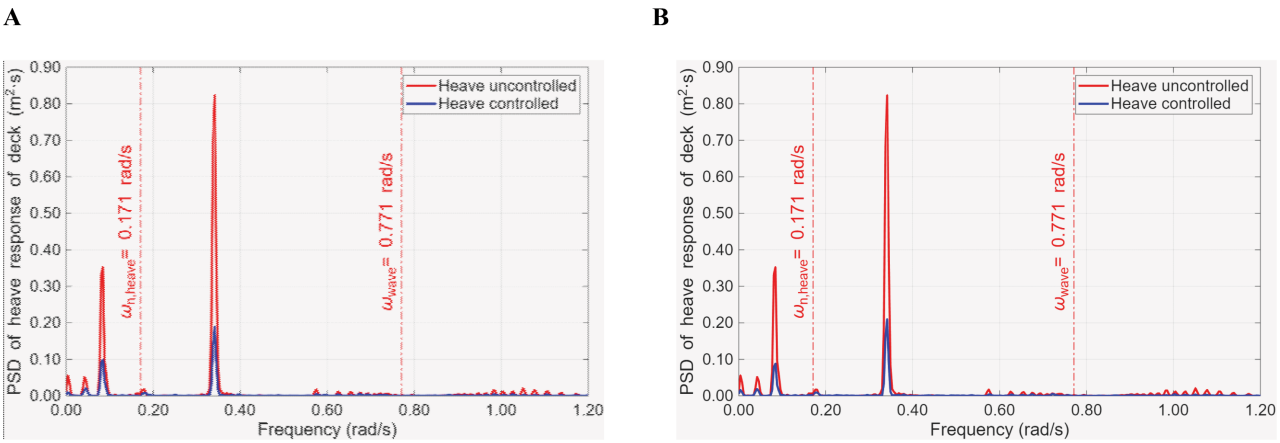

Figure 17. Power spectral density (PSD) of heave response of deck at approach angles (A) 0° and (B) 90° (wave + wind + current; moderate sea state; $H_s = 6.5$ m; $T_z = 8.15$ s)

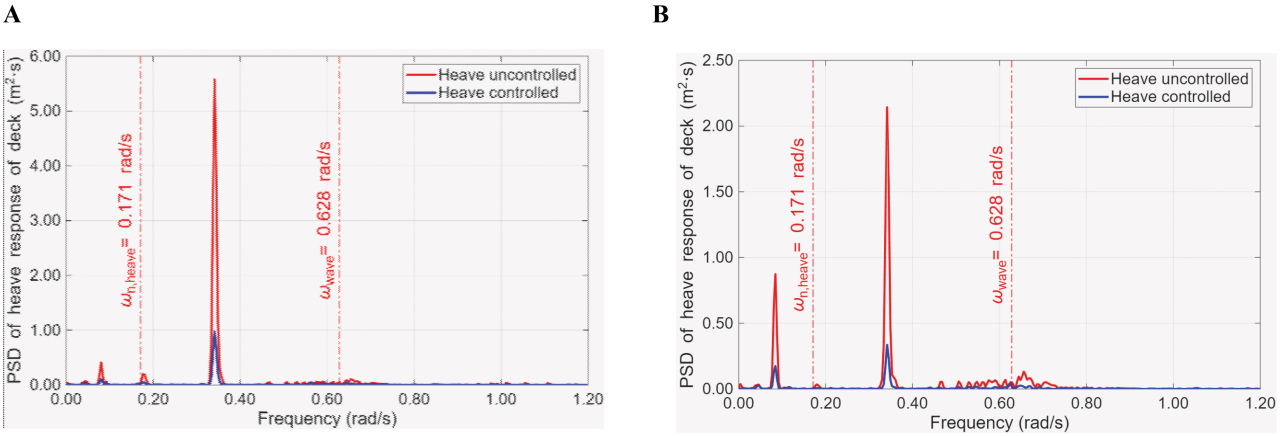

Figure 18. Power spectral density (PSD) of heave response of deck at approach angles (A) 0° and (B) 90° (wave + wind + current; high sea state; $H_s = 6.5$ m; $T_z = 8.15$ s)

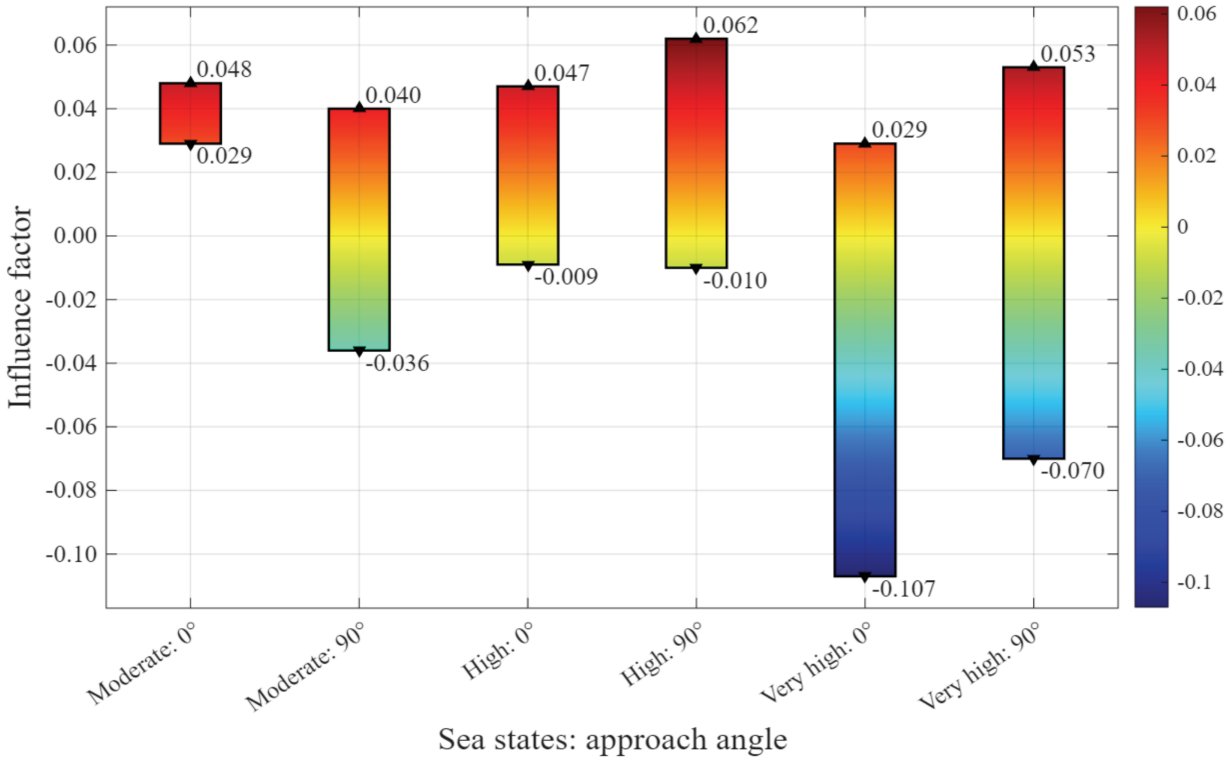

Figure 19. Influence factors for deck heave transformation

Table 7. Statistics of deck heave

Approach angle	Max. (m)	Min. (m)	Mean (m)	RMS (m)	Max. (m)	Min. (m)	Mean (m)	RMS (m)	Reduction (%)
	Uncontrolled				Controlled				
Moderate sea state									
0°	0.513	−0.803	0.000	0.169	0.277	−0.497	0.000	0.096	43.125
90°	0.513	−0.803	0.000	0.169	0.296	−0.461	0.002	0.095	43.601
High sea state									
0°	0.600	−0.825	0.000	0.272	0.552	−0.906	0.003	0.156	42.557
90°	0.655	−0.823	0.000	0.218	0.468	−0.559	0.001	0.127	41.903
Very high sea state									
0°	2.888	−2.873	0.000	1.096	3.479	−3.016	0.061	0.856	21.849
90°	2.646	−2.620	0.000	0.947	4.802	−3.585	0.052	0.946	0.074

Abbreviation: RMS: Root root mean square.

Table 8. Influence factors for deck heave transformation

Sea states	Influence factor range
Moderate: 0°	[0.029, 0.048]
Moderate: 90°	[−0.036, 0.040]
High: 0°	[−0.009, 0.047]
High: 90°	[−0.010, 0.062]
Very high: 0°	[−0.107, 0.029]
Very high: 90°	[−0.070, 0.053]

Figures 17 and 18 show that the heave power spectral density (PSD) peaks for the uncontrolled and MR-RCM-controlled cases occurred at nearly the same frequency, indicating that the platform's natural heave frequency remained unchanged within numerical resolution. Although the natural frequency was around 0.171 rad/s, the PSD peak appeared at a higher frequency because the response spectrum represents the product of the heave response amplitude operator and the wave-energy distribution, which shifts the energy-dominant frequency. Therefore, the MR-RCM did not retune the system but primarily suppressed the peak amplitude. Since the dominant wave-energy frequencies (0.628–0.771 rad/s) remained well separated from the heave-resonance band, the mechanism effectively reduced response levels without introducing any resonance risk under combined environmental loading.

Table 8 and **Figure 19** show the ranges of influence factors for varying sea states and approach angles, providing insights into the interaction between buoyant leg displacements and deck heave.

Under moderate seas, the ranges remained narrow, with 0° [0.029, 0.048] showing positive values that indicate stable proportionality, while 90° [−0.036, 0.040] includes slight negative values, suggesting minor phase-dependent reversals. In high sea states, the ranges broaden, with 0° [−0.009, 0.047] and 90° [−0.010, 0.062], highlighting stronger coupling and possible amplification effects, particularly for oblique loading. The very high sea state exhibited the greatest variability, with 0° [−0.107, 0.029] and 90° [−0.070, 0.053], where negative values dominate. This indicates pronounced nonlinear effects and alternating constructive and destructive contributions of leg motion to deck heave, reducing predictability and emphasizing the importance of RCMs. Thus, the data show that influence factors were more consistent in moderate seas but became increasingly scattered as severity grew.

The observed reductions in peak and RMS responses are expected to reduce cyclic stresses at buoyant leg attachments and tether anchorage points, leading to fatigue-life extension. A detailed fatigue-damage estimation and techno-economic analysis of the MR-RCM is proposed for future work.

The BLSRP operates in a water depth of 600 m, where the tethers provide the dominant restoring stiffness and the mooring response governs global platform behavior. Therefore, soil–pile interaction is not incorporated, and the tether ends were assumed to be fixed at the seabed.

During extreme sea states or power loss, the MR dampers revert to their passive zero-field mode and operate as stable viscous–elastic devices without causing mechanical lock-up or instability. In this fail-safe state, their role shifts from performance enhancement to limiting excessive deformation, ensuring continued safety under survival conditions.

7. Conclusion

The present work presents the development and numerical assessment of a control algorithm for the BLSRP with MR-RCM, implemented using MATLAB simulations and hydrodynamic inputs from AQWA. The numerical calibration ensured that simulated force—displacement and hysteresis loops remained within practical and realistic MR damper capacity for platform leg forces. No physical model testing or validation with offshore installations was performed at this stage. Experimental validation is planned as a continuation of this study to verify the full-scale applicability of the proposed system.

This study demonstrates the effectiveness of a semi-active RCM for the BLSRP using MR dampers modeled through the Bouc–Wen formulation. The study highlights that the MR-RCM can successfully mitigate the inward–outward radial displacements of buoyant legs, which also contribute to deck heave. The transformation procedure developed in this work enables mapping controlled radial responses to deck heave through influence factors that vary with sea state and wave approach angle.

Results show that 30–45% RMS reductions are consistently achieved under moderate and high sea states, with the damper remaining effective even under asymmetric loading. Although the reduction percentage decreased under very high sea states, the MR-RCM continued to prevent uncontrolled escalation of responses, ensuring structural safety. The nonlinear hysteresis loops confirm that MR dampers dissipate substantial energy while adapting to varying excitation levels, balancing robustness and adaptability.

Seabed–foundation interaction is not explicitly modeled in the present study because its influence on platform dynamics is marginal for deep-water conditions.

In this study, JONSWAP spectra and a Gulf of Mexico-type current profile were used as representative conditions. For practical deployment, these must be replaced with site-specific wave spectra, peak periods, and environmental data. The MR-RCM framework remains unchanged, although the Bouc–Wen parameters may be returned to reflect local peak periods and energy levels. Hence, site-specific environmental characterization is required before full-scale application.

While RMS reduction is the key finding, the observed response statistics indicate reduced fatigue damage and enhanced operational reliability. Reduction in heave motion is strongly linked to operational reliability for LNG transfer and reduction of BOG generation.

Overall, the proposed MR-RCM enhances the operational safety and survivability of BLSRPs in deep-water LNG regasification environments. By improving heave control and energy dissipation, the system supports reliable LNG transfer and reduces risks associated with excessive motions. The findings establish MR-based semi-active control as a viable and scalable strategy for offshore platforms, bridging the gap between traditional passive devices and complex active systems.

An Indian patent was granted for the design titled “Damping system for an oil rig” with a design number 426872-001, dated 13/08/2024.

Acknowledgments

The authors gratefully acknowledge the Intellectual Property Rights Cell at the Indian Institute of Technology Madras and the Patent Attorney team for their invaluable support and guidance throughout the patent filing process.

Funding

None.

Conflict of interest

The authors declare they have no competing interests.

Author contributions

Conceptualization: All authors
Data curation: Shyba Arakkan
Formal analysis: Shyba Arakkan
Investigation: Shyba Arakkan
Methodology: Shyba Arakkan
Supervision: Srinivasan Chandrasekaran
Visualization: Shyba Arakkan
Writing–original draft: Shyba Arakkan
Writing–review & editing: Srinivasan Chandrasekaran

Availability of data

The data supporting the findings of this study are presented within the manuscript. Additional or supplementary datasets can be made available by the corresponding author upon reasonable request.

AI tools statement

All authors confirm that no AI tools were used in the preparation of this manuscript.

References

1. Banaszkiewicz T, Chorowski M, Gizicki W, et al. Liquefied natural gas in mobile applications—opportunities and challenges. *Energies*. 2020;13(21):5673. https://www.doi.org/10.3390/en13215673
2. Semaskaite V, Bogdevicius M, Paulauskiene T, Uebe J, Filina-Dawidowicz L. Improvement of regasification process efficiency for floating storage regasification unit. *J Mar Sci Eng*. 2022;10(7):897. https://www.doi.org/10.3390/jmse10070897
3. Giranza MJ, Bergmann A. An economic evaluation of onshore and floating liquefied natural gas receiving terminals: the case study of Indonesia. *IOP Conf Ser Earth Environ Sci*. 2018;150:012026. https://www.doi.org/10.1088/1755-1315/150/1/012026
4. Naveiro M, Romero Gómez M, Arias Fernández I, Baaliña Insua Á. Energy efficiency and environmental measures for floating storage regasification units. *J Nat Gas Sci Eng*. 2021;96:104271. https://www.doi.org/10.1016/j.jngse.2021.104271
5. Naveiro M, Gómez MR, Fernández IA, Gómez J. Exploitation of liquefied natural gas cold energy in floating storage regasification units. *Brodogradnja*. 2021;72(4):47-78. https://www.doi.org/10.21278/brod 72404
6. American Bureau of Shipping (ABS). Guide for Building and Classing – Floating Offshore Liquefied Gas Terminals. ABS; 2018.
7. Det Norske Veritas Germanischer Lloyd. *DNVGL-RP-C205: Environmental Conditions and Environmental Loads*. DNV; 2019. https://www .dnv.com
8. Milioulis K, Bolbot V, Theotokatos G, et al. Safety analysis of a high-pressure fuel gas supply system for LNG-fuelled vessels. *Proc Inst Mech Eng Part M J Eng Marit Environ*. 2022;236(4):1025-1046. https://www.doi.org/10.1177/14750902221078426
9. Chandrasekaran S, Lognath RS. Dynamic analyses of buoyant leg storage and regasification platform: numerical studies. *Mar Syst Ocean Technol*. 2017;12(2):39-48. https://www.doi.org/10.1007/s40868-017-0022-6
10. Chandrasekaran S, Lognath RS. Dynamic analyses of buoyant leg storage regasification platform under regular waves: experimental investigations. *Ships Offshore Struct*. 2017;12(2):227-232. https://www.doi.org/10.1080/17445302.2015.1131006
11. Chandrasekaran S, Kiran PA. Mathieu stability of offshore buoyant leg storage and regasification platform. *Ocean Syst Eng*. 2018;8(3):345-360. https://www.doi.org/10.12989/ose.2018.8.3.345
12. Liang X, Zhang Y, Ge SS, How B, Li D. Dynamic control for LNG carrier with output constraints. *IET Control Theory Appl*. 2022;16(7):729-740. https://www.doi.org/10.1049/cth2.12264
13. Katsimpini P, Papagiannopoulos G, Hatzigeorgiou G. Innovative supplementary dampers for enhancing seismic behavior of structural systems. *Appl Sci*. 2025;15(3):1226. https://www.doi.org/10.3390/app15031226
14. Kandasamy R, Cui F, Townsend N, et al. A review of vibration control methods for marine offshore structures. *Ocean Eng*. 2016;127:279-297. https://www.doi.org/10.1016/j.oceaneng.2016.10.001
15. Suja TP, Chandrasekaran S. Response control of TLP with single tuned mass damper under wind, wave, and current loads. *Mar Technol Res*. 2025;7(1):1-24. https://doi.org/10.33175/mtr.2025.272515
16. You YS, Song KY, Sun MY. Variable natural frequency damper for minimizing response of offshore wind turbine. *J Mar Sci Eng*. 2022;10(7):983. https://www.doi.org/10.3390/jmse10070983
17. Zhang Y, Ma H, Xu J, Su H, Zhang J. Model reference adaptive vibration control of an offshore platform considering marine environment approximation. *J Mar Sci Eng*. 2023;11(1):138. https://www.doi.org/10.3390/jmse11010138
18. Chandrasekaran S, Srivastava G. *Design Aids of Offshore Structures Under Special Environmental Loads Including Fire Resistance*. Springer; 2017. https://www.doi.org/10.1007/978-981-10-7608-4
19. Zakerzadeh M, Mohsenian A, Zakerzadeh MR, Shariat Panahi M, Fakhrzadeh A. Modeling SMA-actuated systems based on the Bouc–Wen hysteresis model and feed-forward neural network. *J Comput Appl Mech*. 2017;48(2):185-200. https://www.doi.org/10.22059/jcamech.2017.234999.151
20. Wang SQ, Li N. Semi-active vibration control for offshore platforms based on LQG method. *J Mar Sci Technol*. 2013;21(5):562-568. https://www.doi.org/10.6119/JMST-012-0917-2
21. Hua D, Liu X, Li Z, Fracz P, Hnydiuk-Stefan A, Li Z. Structural configurations of magnetorheological fluid-based devices: a review. *Front Mater*. 2021;8:640102. https://www.doi.org/10.3389/fmats.2021.640102
22. Ravare D, Mhatre P, Alam H, Sayed A. Magnetorheological damper. *Int J Res Publ Rev*. 2024;5.

https://ijrpr.com/uploads/v5issue3/ijrpr23632.pdf
23. Spencer BF Jr, Dyke SJ, Sain MK, Carlson JD. Phenomenological model for magnetorheological dampers. *J Eng Mech*. 1997;123(3):230-238. https://www.doi.org/10.1061/(asce)0733-9399(1997)123:3(230)
24. Jiang Z, Spencer BF Jr, Sain MK, Carlson JD. Modeling and control of magnetorheological dampers for seismic response reduction. *Smart Mater Struct*. 1996;5(5):566-576. https://www.doi.org/10.1088/0964-1726/5/5/006
25. Ambhore N, Hivarale S, Pangavhane DR. Bouc–Wen model of magnetorheological fluid damper for vibration control. *Int J Eng Res Technol*. 2013;2(2). https://www.ijert.org/research/a-study-of-bouc-wen-model-of-magnetorheological-fluid-damper-for-vibration-control-ijertv2is2296.pdf
26. Heredia PM, Alvarez DA, Bedoya RD. Bouc–Wen class model of hysteresis: evolution, and current state. *Arch Comput Methods Eng*. 2025. https://www.doi.org/10.1007/s11831-025-10301-z
27. Negash BA, You W, Lee J, Lee K. Parameter identification of Bouc–Wen model damper using genetic algorithm. *Adv Mech Eng*. 2020;12(8). https://www.doi.org/10.1177/1687814020950546
28. Oh S, Kim T, Song J. Bouc–Wen class models considering hysteresis mechanism of RC columns. *Int J Non Linear Mech*. 2023;148:104263. https://www.doi.org/10.1016/j.ijnonlinmec.2022.104263
29. Fabrizio M, Lazzari B, Morro A. *Mathematical models and methods for smart materials*. In: Proceedings of the International School on Mathematical Theory in Smart Materials; 2001. Cortona, Italy. World Scientific; 2002. https://www.doi.org/10.1142/5162
30. Hokmabady, H., Mohammadyzadeh, S., Mojtahedi, A. Suppressing structural vibration of a jacket-type platform employing a novel MR-tuned liquid column gas damper. *Ocean Eng*. 2019;180:60-70. https://www.doi.org/10.1016/j.oceaneng.2019.03.055
31. Syed KAA, Kumar D. Response and control of jacket structure with magnetorheological damper at multiple locations. *Ocean Syst Eng*. 2018;8(2):201-221. https://www.doi.org/10.12989/ ose.2018.8.2.201
32. Dutta S, Chakraborty G. Performance analysis of nonlinear vibration isolator with MR damper. *J Sound Vib*. 2014;333(20):5097-5114. https://www.doi.org/10.1016/j.jsv.2014.05.028
33. Høgsberg J, Krenk S. Energy dissipation control of magnetorheological damper. *Probab Eng Mech*. 2008;23(2-3):188-197. https://www.doi.org/10.1016/j.probengmech.2007.12.007
34. Spencer, B.F. Jr, Nagarajaiah, S. State of the art of structural control. *J Struct Eng*. 2003;129(7):845-856. https://www.doi.org/10.1061/(asce)0733–9445
35. Arakkan S, Chandrasekaran S. Mitigating heave response for safer LNG operations: numerical study on offshore BLSRP. In: *Proceedings of the ISOPE Conference*; 2025; ISOPE-I-25-143.
36. Srilekha M, Dutta A. Design and optimization of boil-off gas recondensation by recovering waste cold energy in LNG regasification terminals. *Chem Eng Res Des*. 2024;205:292-300. https://www.doi.org/10.1016/j.cherd.2024.03.041
37. Arakkan S, Chandrasekaran S. *International Conference on Oceanography and Marine Biology*. 2024;63. https://scisynopsisconferences-.com/uploads/conferences/oceanography_73/170497182.pdf
38. Chauhan V, Kumar A, Sham R. Magnetorheological fluids: a comprehensive review. *Manuf Rev*. 2024;11:5. https://www.doi.org/10.1051/mfreview/2024005
39. Bahar A, Pozo F, Meybodi MR, Karami S. Magnetorheological fluid dampers: efficient parametric models. *Struct Control Health Monit*. 2024;2024:6860185. https://www.doi.org/10.1155/2024/6860185
40. Charalampakis AE. Parameters of Bouc–Wen hysteretic Hysteretic model Model revisitedRevisited. 2010. https://www. charalampakis.com/files/c09.pdf
41. Guo Q, Yang X, Li K, Li D. Parameter identification of magnetorheological damper based on particle swarm optimization. *Eng Appl Artif Intell*. 2025;143:110016. https://www.doi.org/10.1016/j.engappai.2025.110016
42. Ismail M, Ikhouane F, Rodellar J. The hysteresis Bouc–Wen model: a survey. *Arch Comput Methods Eng*. 2009;16(2):161-188. https://www.doi.org/10.1007/s11831-009-9031-8
43. Tu J, Li Z, Zhang J, Gao K, Liao J, Gao J. Development, test, and mechanical model of a leakproof magnetorheological damper. *Front Mater*. 2019;6. https://www.doi.org/10.3389/fmats.2019.00118

Shyba Arakkan *is a dedicated research scholar in the Department of Ocean Engineering at the Indian Institute of Technology Madras (IIT Madras), pursuing her Ph.D. under the All-India Council for Technical Education (AICTE) Quality Improvement Programme (QIP). With a strong academic foundation as a faculty member from Government Engineering College Kozhikode, she combines teaching experience with advanced research in offshore structural dynamics. Her*

work centers on the Buoyant Leg Storage and Regasification Platform (BLSRP), focusing on response control mechanisms for motion mitigation under combined wave–wind–current loading. Passionate about innovation and safety in ocean systems, Shyba's interdisciplinary approach—integrating structural dynamics and control theory—reflects her commitment to developing sustainable, resilient offshore technologies and contributing to the future technical experts in the maritime research community.

https://orcid.org/0009-0000-5617-3320 ***Srinivasan Chandrasekaran*** *is a Professor (Higher Academic Grade) in the Department of Ocean Engineering at IIT Madras. He is an expert in structural dynamics of offshore structures, earthquake-resistant design, functionally graded materials (FGM) for offshore topsides, risk-reliability methods, and fire-resistant design of offshore platforms. He has an outstanding academic and research record, with a Google Scholar h-index of 32 and an i-10 index of 92, placing him among the top 2% of world-leading scientists for the past five consecutive years. Professor Chandrasekaran has authored 25 books, published over 107 papers in refereed journals and conferences, and holds 8 granted patents with 10 more filed. He has supervised 27 Ph.D. and 13 M.S. (by Research) students. Recognized for his excellence in teaching and research, he received the Best Reviewer Award from the Korean Society of Steel Structures and the Best Teacher Award from IIT Madras in 2022 and 2025.*

https://orcid.org/0000-0001-8346-5724

An International Journal of Optimization and Control: Theories & Applications
(https://accscience.com/journal/ijocta)